Pedestal Structure Model

J. D. Callen, J. M. Canik, and S. P. Smith

Phys. Rev. Lett. **108**, 245003 — Published 13 June 2012

DOI: 10.1103/PhysRevLett.108.245003

Pedestal Structure Model

J.D. Callen,[1,*] J.M. Canik,[2] and S.P. Smith[3]

[1] *University of Wisconsin, 1500 Engineering Drive, Madison, WI 53706-1609 USA*

[2] *Oak Ridge National Laboratory, P.O. Box 2008, Oak Ridge, TN 37831 USA*

[3] *General Atomics, P.O. Box 85608, San Diego, CA 92186-5608 USA*

Abstract

Predictions are developed for gradients and profiles of the electron density and temperature in tokamak H-mode pedestals that are in transport quasi-equilibrium. They are based on assuming paleoclassical processes provide the irreducible minimum radial plasma transport and dominate in the steep gradient regions of pedestals. The predictions agree (within a factor of about two) with properties of a number of pedestal experimental results.

PACS numbers: 52.55.Fa, 52.25.Fi, 52.55.Dy, 52.25.Xz, 52.55.Rk

Plasmas with large gradients in their edge pedestals (outer few % of the plasma radius) occur in fusion-relevant high- (H-) confinement mode tokamak plasmas. Substantial pedestal heights are critical [1] for achieving high fusion power in ITER [2]. Plasma transport and its role in H-mode pedestals are not presently understood.

An extensive study of plasma transport in a DIII-D H-mode pedestal [3] indicated paleoclassical plasma transport [4, 5] may play a significant role there. This paper develops and tests the fundamental predictions of a paleoclassical-based model for the "pedestal structure" in the edge of H-mode plasmas. A comprehensive description, more predictions and implications of the model are presented in [6]. Additional tests are presented in [6–8].

The model predictions will be illustrated by comparison to plasma transport quasi-equilibrium profiles in the edge of the low collisionality DIII-D tokamak discharge 98889 [3] shown in Fig. 1. The radial coordinate $\rho_N \equiv \rho/a$ is the normalized minor radius in terms of the toroidal-flux-based radial coordinate ρ (m). The separatrix is at $\rho_N = 1$ ($a \simeq 0.77$ m) in this lower single null diverted plasma. Key edge plasma regions are the core (I) and steep gradient parts (II and III) of the pedestal.

The key assumption used in this model is that paleoclassical processes dominate all plasma transport channels in the steep gradient region of the pedestal. While fluctuations are usually present in pedestals and may peak where the plasma pressure gradient is largest, they will be assumed to be too small to induce the dominant plasma transport in regions II and III.

The initial paleoclassical papers [4, 5] were based on a key hypothesis that charged particles diffuse radially along with thin annuli of poloidal magnetic flux in resistive, current-

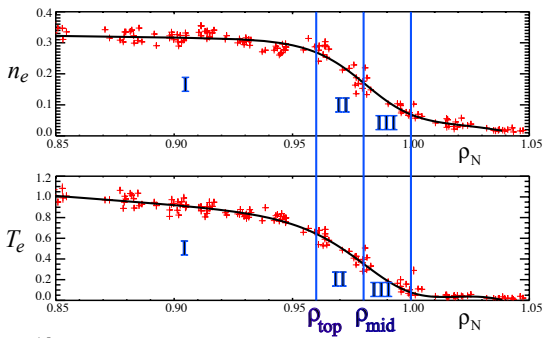

FIG. 1. Electron density n_e ($\times 10^{20}$ m^{-3}) and temperature T_e (keV) profiles in edge of DIII-D discharge 98889 [3]. Pedestal top is at $\rho_{\rm top} = 0.96\,a$ and its mid-point is at $\rho_{\rm mid} = 0.98\,a$.

carrying toroidal plasmas. That is, they diffuse radially with the resistivity-induced magnetic field diffusivity $D_\eta = \eta/\mu_0$. This hypothesis was later shown [9] to result from transforming the drift-kinetic equation from laboratory to poloidal flux coordinates, upon which Grad-Shafranov equilibria, neoclassical transport theory and gyrokinetic-based anomalous transport analyses are based. A Comment [10] on [9] asserted the effects "appear to lack a systematic basis." The Response [11] provided a systematic multiple-time-scale analysis of electron guiding center motion that produces these effects.

Paleoclassical electron heat transport approximately agrees with results from many ohmic-level [$T_e \lesssim B(\mathrm{T})^{2/3} a(\mathrm{m})^{1/2}$ keV] toroidal plasmas [12] (tokamaks, STs, RFPs, spheromaks), in electron-cyclotron (EC) heated plasmas in RTP [13] and in tokamak H-mode pedestals [3, 12]. These results are consistent with it providing the minimum level of electron heat transport.

The fundamental paleoclassical parameter is [5, 11, 14] the poloidal magnetic flux diffusivity $D_\eta \equiv \eta_\parallel^{\rm nc}/\mu_0$ induced by the parallel neoclassical resistivity $\eta_\parallel^{\rm nc}$. An approximate formula for D_η ($\mathrm{m^2\,s^{-1}}$) in typical H-mode pedestals in which $Z_{\rm eff} \equiv \sum_i n_i Z_i^2/n_e \simeq 1.5$–$3$ can be developed [6] that includes parallel friction (Spitzer) and trapped-particle-induced viscosity (f_t, ν_{*e}) effects:

$$D_\eta \simeq \frac{1300\, Z_{\rm eff}}{[T_e(\mathrm{eV})]^{3/2}} \left(0.41 + \frac{1.2 (f_t/f_c)/(1+\nu_e/\omega_{te})}{1+\nu_{*e}^{1/2} + 2\,\nu_{*e}} \right). \tag{1}$$

Here, f_c is the flow-weighted fraction [15] of circulating (untrapped) particles with Padé approximate [16]

$$f_c \simeq \frac{(1-\epsilon^2)^{-1/2}\,(1-\epsilon)^2}{1+1.46\,\epsilon^{1/2}+0.2\,\epsilon} \overset{\epsilon\ll 1}{\simeq} 1 - 1.46\,\epsilon^{1/2} + \mathcal{O}(\epsilon), \tag{2}$$

in which $\epsilon \equiv (B_{\rm max} - B_{\rm min})/(B_{\rm max} + B_{\rm min}) \simeq r_M/R_0$ is the local magnetic inverse aspect ratio. The fraction of trapped particles is $f_t \equiv 1 - f_c$. Finally, the neoclassical electron collisionality parameter is in general [6, 15, 17]

$$\nu_{*e} \equiv \frac{(f_t/f_c)\,\nu_e}{2.92\, v_{Te}} \frac{\langle B^2\rangle/R_0 q}{\langle (\hat{\mathbf{b}}\cdot\boldsymbol{\nabla} B)^2\rangle} \simeq \frac{(f_t/f_c) R_0 q}{1.46\,\epsilon^2 \lambda_e} \overset{\epsilon\ll 1}{\simeq} \frac{\nu_e}{\epsilon^{3/2}\omega_{te}}, \tag{3}$$

in which the electron Coulomb collision length is

$$\lambda_e \equiv \frac{v_{Te}}{\nu_e} \simeq 1.3\times 10^{16}\, \frac{[T_e(\mathrm{eV})]^2}{Z_{\rm eff}\, n_e(\mathrm{m^{-3}})}\ \ \mathrm{m}. \tag{4}$$

TABLE I. Key parameters for the DIII-D 98889 pedestal [3].

Parameter	at $\rho_{\rm top}$	at $\rho_{\rm mid}$	at $\rho_{\rm sep} = a$
T_e(eV)	666	352	89
$n_e/10^{19}{\rm m}^{-3}$	2.76	1.77	0.77
$Z_{\rm eff}$	2.83	2.6	1.9
$\epsilon \equiv r_M/R_0$	0.347	0.352	0.356
f_t/f_c	3.24	3.31	3.38
λ_e(m)	74	35	7
$R_0 q/\lambda_e \equiv \nu_e/\omega_{te}$	0.10	0.21	∞
ν_{*e}	1.9	3.9	∞
$D_\eta \equiv \eta_\parallel^{\rm nc}/\mu_0$ $({\rm m}^2\,{\rm s}^{-1})$	0.21	0.36	1.2

Table I provides values of these key parameters for the data shown in Fig. 1 for which $r_M(\rho_{\rm mid}) \simeq 0.6$ m, $R_0 \simeq 1.7$ m, and the "safety factor" $q(\rho_{\rm mid}) \simeq 4.5$. On the separatrix $q \to \infty$. Because the fraction of trapped particles is large in the pedestal [$f_t(\rho_{\rm mid}) \simeq 0.77$, $f_c(\rho_{\rm mid}) \simeq 0.23$], the relevant electron collisionality parameter $\nu_{*e}(\rho_{\rm mid}) \simeq 3.9$ is a factor of about 4 larger than the result from the usual low aspect ratio formula $\nu_e/\epsilon^{3/2}\omega_{te}$, which is 1.0 at $\rho_{\rm mid}$. Thus, because of the low aspect ratio ($1/\epsilon \sim 2.8$ in DIII-D), pedestal plasmas are usually not in the low collisionality "banana" regime; rather, they are typically in the higher collisionality plateau or even Pfirsch-Schlüter regimes. Electron viscosity (f_t, ν_{*e}) effects are significant and vary in the pedestal; the ν_{*e}-dependent term in (1) increases from 0 at the separatrix to 0.3 at $\rho_{\rm mid}$ and 0.56 at $\rho_{\rm top}$.

In plasma transport quasi-equilibria shortly after ($\gtrsim$ 10 ms) an L-H transition or just before an edge-localized-mode (ELM) such as those discussed in [3, 18], the "steady-state" ($\partial/\partial t \to 0$) flux-surface-averaged (FSA) density transport equation is [14]

$$\langle \boldsymbol{\nabla}\cdot\boldsymbol{\Gamma}\rangle \;\equiv\; \frac{1}{V'}\,\frac{d}{d\rho}(V'\Gamma) \;=\; \langle S_n\rangle. \tag{5}$$

Here, $\boldsymbol{\Gamma}$ is the density flux, $\Gamma \equiv \langle \boldsymbol{\Gamma}\cdot\boldsymbol{\nabla}\rho\rangle$ the FSA radial flux, $\langle S_n\rangle$ the net FSA density source and $V' \equiv dV/d\rho$ $({\rm m}^2)$ where $V(\rho)$ $({\rm m}^3)$ is the volume of the ρ flux surface.

The FSA paleoclassical radial density flux is [14]

$$\Gamma^{\rm pc} = -\,\frac{1}{V'}\,\frac{d}{d\rho}(V'\bar{D}_\eta\, n) = -\,\bar{D}_\eta\,\frac{dn}{d\rho} \;+\; n\,V_{\rm pinch}. \tag{6}$$

The $\Gamma^{\rm pc}$ includes a pinch flux, which results from particle guiding centers only diffusing radially because the $\mathcal{O}\{\epsilon^2\}$ Fokker-Planck drag-type term is negligible [5, 11]. The pinch flow velocity (m s^{-1}) is usually inward (i.e., < 0); its definition is

$$V_{\rm pinch} \equiv -\frac{1}{V'}\frac{d}{d\rho}(V'\bar{D}_\eta). \tag{7}$$

Here, the geometric factor [5] $a^2/\bar{a}^2 \equiv \langle|\boldsymbol{\nabla}\rho|^2/R^2\rangle/\langle R^{-2}\rangle$ ($\simeq 1.6$ for the 98889 pedestal [3]) has been incorporated in the magnetic field diffusivity for simplicity of notation:

$$\bar{D}_\eta \equiv \frac{a^2}{\bar{a}^2}D_\eta, \quad \text{geometrically effective } D_\eta,\ \text{m}^2\,\text{s}^{-1}. \tag{8}$$

Assuming the total density flux Γ is just $\Gamma^{\rm pc}$, multiplying (5) by $dV \equiv V'd\rho$ and integrating radially from the ρ flux surface to the separatrix ($\rho_{\rm sep} \equiv a$) yields an equation for the radial flow of charged particles (s^{-1}):

$$-\left[\frac{d}{d\rho}(V'\bar{D}_\eta\, n)\right]_\rho = \dot{N}(\rho). \tag{9}$$

Here, $\dot{N}(\rho)$ is the number of particles flowing across the ρ surface per second: $\dot{N}(\rho) \equiv \dot{N}(a) - \int_\rho^a d\hat{\rho}\, V'(\hat{\rho})\,\langle S_n(\hat{\rho})\rangle$.

Deuteron and impurity (e.g., carbon) densities in pedestals are influenced by complicated differing source, ionization and neoclassical pinch-type effects. Thus, the simpler electron density equation is solved. Integrating (9) radially from ρ to a reference radius $\rho_{\rm ref}$ yields

$$n_e(\rho)\,\bar{D}_\eta(\rho)\,V'(\rho) = [n_e\,\bar{D}_\eta\,V']_{\rho_{\rm ref}} + \int_\rho^{\rho_{\rm ref}} d\hat{\rho}\,\dot{N}_e(\hat{\rho}). \tag{10}$$

The density source effect is often small. For example, at the mid-point of the 98889 pedestal [3] the relative magnitude of the fueling between $\rho_{\rm mid} = 0.98\,a$ and $\rho_{\rm ref} \to a$ is $\lesssim 0.02\,a\,\dot{N}_e(a)/[n_e\bar{D}_\eta V']_{\rho_{\rm mid}} \simeq 0.07$ since in 98889 [3] $\dot{N}_e(a) \simeq 2\times10^{21}$ s^{-1} and $V' \simeq (\rho/a)(43.4)$ m^2.

Neglecting fueling and variations in V', $a^2/\bar{a}^2$, (10) becomes

$$n_e(\rho)\,D_\eta(\rho) \simeq [n_e D_\eta]_{\rho_{\rm ref}} = \text{constant}. \tag{11}$$

This relation predicts $n_e(\rho) \propto 1/D_\eta(\rho)$; i.e., n_e increases strongly from the separatrix inward as $D_\eta \propto 1/T_e^{3/2}$ decreases. It also implies the top of the n_e profile occurs where T_e "saturates" (for $\rho \lesssim \rho_{\rm top} = 0.96\,a$ in Fig. 1). If D_η were spatially constant, (11) would predict $n_e(\rho) =$ constant in the pedestal, i.e., no density pedestal.

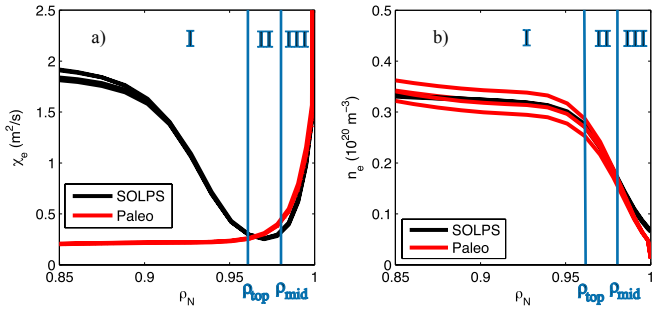

FIG. 2. Comparison of paleoclassical-based pedestal structure model predictions (red) to SOLPS interpretive modeling [7] (black) for 4 carbon transport models that result in slightly different $Z_{\rm eff}$ profiles for the DIII-D 98889 pedestal [3]: a) effective electron heat diffusivity χ_e and b) density n_e profiles.

The relation in (11) indicates the density profile that produces a small net electron paleoclassical density flux $\Gamma_e^{\rm pc}$ in (6) — by nearly balancing the outward diffusive density flux with a large inward pinch flux. This scenario is precisely what was concluded from a pioneering interpretive analysis [19] of the ion density pinch and diffusivity in the 98889 pedestal; paleoclassical predictions for D_η and $V_{\rm pinch}$ are consistent with the values and profiles obtained with that analysis (see Figs. 25, 26 in [3]).

Differentiating (11) with respect to ρ yields a lowest order prediction for the electron density gradient scale length: $1/L_{n_e} = 1/L_\eta$ in which $1/L_{n_e} \equiv -d\ln n_e/d\rho$ and $1/L_\eta \equiv d\ln D_\eta/d\rho$. The tanh fit [3] "width" of the density pedestal is approximately $2L_{n_e}$. At $\rho_{\rm mid}$ in 98889 $L_\eta/a \simeq 0.02$ is slightly smaller than the experimentally-inferred width of $L_{n_e}^{\rm exp}/a \simeq 0.0285$ (see Fig. 9b in [3]).

The magnetic field diffusivity D_η varies as $Z_{\rm eff}/T_e^{3/2}$ times a function of the electron collisionality parameter $\nu_{*e}(T_e, Z_{\rm eff}, n_e)$. Thus, it depends strongly on the yet to be determined T_e profile. Since D_η depends mainly on T_e, the n_e and T_e profiles should be "aligned" (i.e., strongly correlated). Edge fueling decreases the pedestal density "width" slightly [20] while additional collision- or turbulence-induced density transport can increase it [6].

Figure 2b shows the n_e profile predicted by (11) (here normalized to the average of the pedestal experimental data) compares favorably to the experimental n_e profile in 98889. The n_e profiles are compared instead of effective density diffusivities $D_{\rm eff} \sim \dot{N}/[V'(-dn_e/d\rho)]$ because the diffusion and pinch terms in (6) nearly cancel.

A comprehensive study [8] of $n_e^{\rm pc}(\rho_{\rm mid})$ predicted by (10) with $\rho_{\rm ref} = a$ using the DIII-D pedestal database (> 200 time slices) found $n_e^{\rm pc}(\rho_{\rm mid})/n_e^{\rm exp}(\rho_{\rm mid}) \simeq 2.1 \pm 0.7$ with a correlation coefficient of 0.89. Fueling effects were only about 5%. While this pedestal structure model provided the minimum density transport, the average overprediction of $n_e(\rho_{\rm mid})$ by a factor of about two indicates some modest additional density transport apparently occurs in most DIII-D pedestals.

The steady-state FSA electron energy transport equation analogous to (5) for the density is [5, 14]

$$\langle \boldsymbol{\nabla}\cdot \mathbf{q}_e^{\rm pc}\rangle \,+\, \frac{1}{V'}\,\frac{d}{d\rho}[V'(\Upsilon_e + \frac{5}{2}\,T_e\,\Gamma)] \,=\, Q_e^{\rm net}. \tag{12}$$

Here, $\mathbf{q}_e^{\rm pc}$ is the paleoclassical electron heat flux, $\Upsilon_e \equiv \langle \mathbf{q}_e\cdot\boldsymbol{\nabla}\rho\rangle$ is the FSA of any additional radial electron heat fluxes and $Q_e^{\rm net}$ is the net FSA electron energy source.

The FSA paleoclassical radial electron heat transport operator is not in standard form, but is (Eq. (142) in [5])

$$\langle \boldsymbol{\nabla}\cdot \mathbf{q}_e^{\rm pc}\rangle = -\,\frac{M+1}{V'}\,\frac{d^2}{d\rho^2}\left(V'\bar{D}_\eta\,\frac{3}{2}\,n_eT_e\right),\ {\rm W\,m^{-3}}. \tag{13}$$

The M factor is caused by helically-resonant radial electron heat transport contributions [5] near medium order rational surfaces. In H-mode pedestals it is roughly $M \simeq \lambda_e/(\pi R_0 q)$ [5], which in the 98889 pedestal is about 3.1 at $\rho_{\rm top}$, 1.5 at $\rho_{\rm mid}$ and zero at a [6].

Multiplying (12) by $V'/(M+1)$, neglecting other electron heat fluxes in the pedestal, integrating radially from ρ to a and using (9) for $-\,[(d/d\rho)(V'\bar{D}_\eta n_e)]_\rho$ yields an equation for electron heat flow (W):

$$-\,[V'\bar{D}_\eta\,n_e]\,\frac{3}{2}\,\frac{dT_e}{d\rho} + \frac{3}{2}\dot{N}_eT_e \;=\; P_e(\rho). \tag{14}$$

Here, $P_e(\rho)$ is an effective conductive electron heat flow (W) through the ρ flux surface:

$$P_e(\rho) \equiv P_e(a) - \int_\rho^a \frac{d\hat{\rho}\,V'(\hat{\rho})}{M(\hat{\rho})+1}\left[Q_e^{\rm net} - \frac{1}{V'}\frac{d}{d\rho}\left(V'\frac{5}{2}T_e\Gamma\right)\right]_{\hat{\rho}}. \tag{15}$$

This is the electron heat flow through the separatrix $P_e(a) \equiv -\,[(d/d\rho)(V'\bar{D}_\eta(3/2)n_eT_e)]_a$ (since $M \to 0$ at the separatrix) minus typically small [3] corrections due to electron heating $Q_e^{\rm net}$ and convective electron heat flow between ρ and a. The $\dot{N}_e$ fueling term in (14) is often negligible compared to conductive electron heat flow through the pedestal: $(3/2)\dot{N}_eT_e/P_e \lesssim 0.026$ in the 98889 pedestal [3] where $P_e(\rho_{\rm mid}) \simeq 1.65\times 10^6$ W.

Neglecting electron heat losses due to the fueling $\dot{N}_e$, the predicted electron temperature gradient is thus

$$-\frac{dT_e}{d\rho} = \frac{P_e}{(3/2)\,[V'\bar{D}_\eta\, n_e]} \simeq \text{spatially constant.} \tag{16}$$

The gradient of T_e is predicted to be approximately constant in the pedestal's steep gradient region (II and III in Fig. 1) because the conductive electron heat flow is often nearly constant in the pedestal (i.e., $P_e(\rho) \simeq P_e(a)$ — see Figs. 4a and 5a in [3]) and from (11) $[V'\bar{D}_\eta\, n_e]$ is predicted to be nearly constant in H-mode pedestals. The T_e profiles in tokamak H-mode plasmas frequently exhibit roughly spatially constant T_e gradients in the steep gradient region of their pedestals, e.g., as in Fig. 1; however, significant measurement error bars prevent definitive conclusions about this prediction's veracity.

Dividing (16) by T_e and multiplying by a yields a prediction for the normalized T_e gradient scale length at any ρ in the pedestal steep gradient region (II, III): $L_{T_e}/a \equiv (-\,a\,d\ln T_e/d\rho)^{-1} = (3/2)\,[V'\bar{D}_\eta n_e]\,T_e/(a\,P_e)$. At the mid-point $\rho_{\rm mid}$ of the 98889 pedestal, this predicts $[L_{T_e}/a]_{\rho_{\rm mid}} \simeq 0.029$ compared to the experimentally-inferred width of $[L_{T_e}/a]^{\rm exp}_{\rho_{\rm mid}} \simeq 0.02$ (see Fig. 9b in [3]).

Using the $dT_e/d\rho$ prediction in (16), in the pedestal the effective electron heat diffusivity is (Eq. (13) in [3])

$$\chi^{\rm pc}_{e\,\rm eff} \equiv \frac{P_e}{V'\langle|\boldsymbol{\nabla}\rho|^2\,\rangle(-\,n_e dT_e/d\rho)} = \frac{a^2/\bar{a}^2}{\langle|\boldsymbol{\nabla}\rho|^2\rangle}\,\frac{3}{2}\,D_\eta. \tag{17}$$

In the steep gradient region of the 98889 pedestal, $a^2/\bar{a}^2 \simeq 1.6$ and $\langle|\boldsymbol{\nabla}\rho|^2\rangle \simeq 2$; thus, the model prediction is that $\chi^{\rm pc}_{e\,\rm eff} \simeq 1.2\,D_\eta$ there. This $\chi^{\rm pc}_{e\,\rm eff}$ prediction in the pedestal region is different from the usual local paleoclassical estimate [5] of $\chi^{\rm pc}_e \simeq (3/2)(M{+}1)D_\eta$ because of the non-standard form of the paleoclassical electron heat transport operator shown in (13) and because there is very little local electron heating in the pedestal — electron heat mostly just flows radially through the pedestal.

Figure 2a shows the pedestal structure model prediction in (17) agrees well with the χ_e profile in the pedestal steep gradient region (II and III in Figs. 1,2). The electron heat transport is apparently "anomalous" from the pedestal top inward (i.e., for $\rho_N < 0.96$, I in Figs. 1,2).

Similar modeling results were obtained [7] for the n_e and χ_e profiles using this model for plasmas in NSTX without and with lithium-coated plasma-facing components, which strongly modified the pedestal carbon density and $Z_{\rm eff}$ profiles in the pedestal. In those

pedestals $f_t/f_c \simeq 0.93/0.07 \sim 13$ is very large. No anomalous electron heat transport was needed for the case with lithium in to $\Psi_N \simeq 0.82$ (see Fig. 13a in [7]).

A comprehensive study [8] of the $dT_e^{\rm pc}/d\rho$ predicted by (16) using the DIII-D pedestal database (> 200 time slices) found $[(dT_e^{\rm pc}/d\rho)/(dT_e^{\rm exp}/d\rho)]_{\rho_{\rm mid}} \simeq 1.7 \pm 1.1$ with a correlation coefficient of 0.55. Thus, the minimum level of T_e transport used in obtaining (16) is within experimental uncertainties; but additional electron heat transport is apparently operative at high β_p and low ν_{*e} [8].

Only a small anomalous $D^{\rm an}$ is required to reduce the pedestal n_e gradient while a much larger $\chi_e^{\rm an}$ is required to reduce the pedestal T_e gradient [6]. The $D_{\rm eff}$ at $\rho_{\rm mid}$ in 98889 can be estimated two ways: from the $\dot{N}_e$ source, $D_{\rm eff} \simeq 0.02$–$0.05\ {\rm m^2\,s^{-1}}$ (see Fig. 24 in [3]), and from what is needed [6] to obtain $L_{n_e}^{\rm exp}$, $D_{\rm eff} \sim 0.12\ {\rm m^2\,s^{-1}}$. At $\rho_{\rm mid}$ in the 98889 pedestal $D^{\rm an} \gtrsim 0.02$–$0.12\ {\rm m^2\,s^{-1}}$ [3, 6] can modify the n_e gradient while T_e profile effects are small unless [6] $\chi_e^{\rm an} \gtrsim [(a^2/\bar{a}^2)/\langle|\boldsymbol{\nabla}\rho|^2\rangle]\,\chi_e^{\rm pc} \sim 1\ {\rm m^2\,s^{-1}}$. This typical order of magnitude greater sensitivity to anomalous density transport than to electron heat transport may provide an interpretation for ELM-free EHO-induced Quiescent H- (QH-) modes in DIII-D [21] and EDA H-modes in C-Mod [22] that have quasi-coherent magnetic fluctuations in their pedestals. Also, it provides a possible interpretation for the C-Mod I-mode regime [22, 23] in which the n_e profile has no edge transport barrier or pedestal (i.e., is L-mode like) but the T_e profile exhibits a normal H-mode-like pedestal in the presence of weakly coherent high frequency modes.

Paleoclassical processes apparently provide the minimum level of n_e and T_e transport in pedestals. They are the basis for the pedestal structure model developed and tested against experimental data in this paper. The new paradigms posited by this pedestal structure model are: 1) the electron temperature gradient in the pedestal increases to (16) so the large electron heat flux from the core can be carried through the pedestal via paleoclassical radial electron heat transport; and 2) the pedestal density profile adjusts to (11) to minimize the net paleoclassical density transport through the pedestal.

The authors are grateful to the co-authors in [3], especially R.J. Groebner and T.H. Osborne, for development and discussions of the DIII-D 98889 pedestal data. This research was supported by DoE grant DE-FG02-92ER54139 (UW) and contracts DE-AC05-00OR22725 (ORNL) and DE-FC02-04ER54698 (GA).

* callen@engr.wisc.edu; http://www.cae.wisc.edu/∼callen

[1] J.E. Kinsey et al., Nucl. Fusion **43**, 1845 (2003).

[2] R. Aymar et al., Nucl. Fusion **41**, 1301 (2001).

[3] J.D. Callen, R.J. Groebner, T.H. Osborne, J.M. Canik, L.W. Owen, A.Y. Pankin, T. Rafiq, T.D. Rognlien and W.M. Stacey, Nucl. Fusion **50**, 064004 (2010).

[4] J.D. Callen, Phys. Rev. Lett. **94**, 055002 (2005).

[5] J.D. Callen, Phys. Plasmas **12**, 092512 (2005).

[6] J.D. Callen, "Model For Pedestal Structure," report UW-CPTC 11-4, July, 2011 (submitted to Phys. Plasmas), available via `http://www.cptc.wisc.edu`.

[7] J.M. Canik et al., Phys. Plasmas **18**, 056118 (2011).

[8] S.P. Smith et al., "Comparing paleoclassical based pedestal model predictions of electron quantities to measured DIII-D H-mode profiles," H-mode workshop, 10-12 October, Oxford, UK (being submitted to Nuclear Fusion).

[9] J.D. Callen, Phys. Plasmas **14**, 040701 (2007)

[10] J.W. Connor, R.J. Hastie and J.B. Taylor, Phys. Plasmas **15**, 014701 (2008).

[11] J.D. Callen, Phys. Plasmas **15**, 014702 (2008).

[12] J.D. Callen et al., Nucl. Fusion **47**, 1449 (2007).

[13] G.M.D. Hogeweij, J.D. Callen, RTP team and TEXTOR team, Plasma Phys. Control. Fusion **50**, 065011 (2008).

[14] J.D. Callen, A.J. Cole, and C.C. Hegna, Phys. Plasmas **16**, 082504 (2009); J.D. Callen, C.C. Hegna, and A.J. Cole, Phys. Plasmas **17**, 056113 (2010).

[15] S.P. Hirshman and D.J. Sigmar, Nucl. Fusion **21**, 1079 (1981).

[16] C.T. Hsu, K.C. Shaing, R.P. Gormley and D.J. Sigmar, Phys. Fluids B **4**, 4023 (1992).

[17] Y.B. Kim, P.H. Diamond and R.J. Groebner, Phys. Fluids B **3**, 2050 (1991).

[18] R.J. Groebner, T.H. Osborne, A.W. Leonard and M.E. Fenstermacher, Nucl. Fusion **49**, 045013 (2009).

[19] W.M. Stacey and R.J. Groebner, Phys. Plasmas **16**, 102504 (2009).

[20] R.J. Groebner et al., Phys. Plasmas **9**, 2134 (2002).

[21] K.H. Burrell et al., Phys. Plasmas **12**, 056121 (2005).

[22] R.M. McDermott et al., Phys. Plasmas **16**, 056103 (2009).

[23] D.G. Whyte et al., Nucl. Fusion **50**, 105005 (2010).